CHINESE OPTICS LETTERS

Vol. 20, No. 4 | April 2022

Direct generation of a stable multi-beam pulsed 355 nm UV laser based on a micro-lens array

Jiao Wei (魏 娇)[1,2], Pixian Jin (靳丕铦)[1,2], Xuechen Cao (曹雪辰)[1], Jing Su (苏 静)[1,2], Huadong Lu (卢华东)[1,2*], and Kunchi Peng (彭堃墀)[1,2]

[1] State Key Laboratory of Quantum Optics and Quantum Optics Devices, Institute of Opto-Electronics, Shanxi University, Taiyuan 030006, China

[2] Collaborative Innovation Center of Extreme Optics, Shanxi University, Taiyuan 030006, China

*Corresponding author: luhuadong@sxu.edu.cn

Received December 18, 2021 | Accepted February 17, 2022 | Posted Online March 9, 2022

Multi-beam laser processing is a very popular method to improve processing efficiency. For this purpose, a compact and stable multi-beam pulsed 355 nm ultraviolet (UV) laser based on a micro-lens array (MLA) is presented in this Letter. It is worth noting that the MLA is employed to act as the spatial splitter as well as the coupling lens. With assistance of the MLA, the 1064 nm laser and 532 nm laser are divided into four sub-beams and focused at different areas of the third-harmonic generation (THG) crystal. As a result, the multi-beam pulsed 355 nm UV laser is successfully generated inside the THG crystal. The measured pulse widths of four sub-beams are shorter than 9 ns. Especially, the generated four sub-beams have good long-term power stability benefitting from the employed MLA. We believe that the generated stable multi-beam 355 nm UV laser can meet the requirement of high-efficiency laser processing, and the presented method can also pave the way to generate stable and long-lived multi-beam UV lasers.

Keywords: micro-lens array; third-harmonic generation; direct generation; pulsed UV laser.

DOI: 10.3788/COL202220.041405

1. Introduction

The ultraviolet (UV) laser has been a kind of promising laser source in the industrial processing fields including circuit board manufacturing[1], semiconductor wafer scribing and dicing[2], micro-via drilling[3], and laser patterning on glass[4] owing to its high energy of the single photon, excellent focusing performance, and superior resolution. Moreover, because of the high-energy characteristic of the single photon, the UV laser can directly disrupt the chemical bonds of material atoms and effectively reduce the thermal diffusion in the course of processing[5,6], which makes the UV laser able to be employed in non-metallic materials processing. So far, the most popular method for achieving the high-quality pulsed 355 nm UV laser is cascaded second-harmonic generation (SHG) and third-harmonic generation (THG) from the fundamental-wave 1064 nm laser. As early as 1989, Chen *et al.* already demonstrated the generation of the 355 nm UV laser with the assistance of the THG crystal LiB_3O_5 (LBO), and the conversion efficiency of 60% was achieved[7,8], which paved the way to attain the UV laser with the high output power. In order to further scale up the output power of the 355 nm UV laser, the cascaded master oscillator power amplifier (MOPA) configuration was employed to amplify the power of the fundamental-wave 1064 nm laser. On this basis, Chen *et al.* realized the highest average power of a 43.7 W pulsed 355 nm UV laser in 2013 by combining the hybrid fiber-MOPA-bulk amplifiers with the walk-off compensated LBO[9]. In addition, many novel crystals were also developed and broadly applied in the THG process to generate the 355 nm UV laser, such as $La_2CaB_{10}O_{19}$[10], BiB_3O_6[11], and $K_3B_6O_{12}Br$[12]. However, so far, the LBO crystal was still the most popular THG crystal because of its relatively large acceptance angle and the weak walk-off effect. With the output power improvement of the 355 nm UV laser, the challenge we had to face was the short lifetime of the achieved laser sources since a SiO_2-amorphous layer would significantly grow on the surface of the LBO crystal when the LBO crystal was exposed to the long-term high power density of the pulsed 355 nm UV laser, which gave rise to the catastrophic break-down of the LBO surface[13]. Though Hong *et al.* improved the surface life of the LBO crystal by super-polishing the output surface to sub-nanometer scale supersmooth roughness in 2013[14], the catastrophic break-down of the LBO surface still occurred only if the power density of the UV laser reached up to its damage threshold. Therefore, how to improve the lifetime of the LBO crystal to satisfy the demand of industrial processing was a critical issue. For another, in order to improve the efficiency of the laser processing, multi-points processing at a time was proposed, which was achieved by

transforming one UV laser beam to multi-beam output. For this purpose, the spatial light modulator (SLM)[15,16] or the diffraction optical element (DOE) beam splitter[17] was employed after the generation of the UV laser from the THG crystal, which would directly complicate the system and introduce the attenuation of output power. The THG crystal still suffered from the illumination of the high power intensity of the 355 nm UV laser, which did nothing for improving the lifetimes of the THG LBO crystal as well as the obtained 355 nm UV laser. Therefore, how to directly generate a multi-beam 355 nm UV laser and prevent the crystal from the radiation of powerful pulse UV laser was also a critical issue. In this Letter, we developed a novel method to directly generate a stable multi-beam pulsed 355 nm UV laser with the assistance of a micro-lens array (MLA), where the MLA was placed in front of the THG crystal to divide and focus the generated 532 nm laser and the residual 1064 nm laser into four sub-beams at different areas on the cross section of the LBO crystal. Because the power density of every sub-beam inside LBO crystal was significantly decreased, the stability and lifetime of the laser system were both improved. Finally, a four-beam pulsed 355 nm UV laser was obtained at the repetition rates of 46.6 kHz, where the average powers of four UV laser beams were 269 mW (Laser I), 179 mW (Laser II), 217 mW (Laser III), and 410 mW (Laser IV), respectively. The measured pulse widths of four sub-beams were shorter than 9 ns.

2. Experimental Design

In order to achieve the goal mentioned above, we designed and built a 355 nm UV laser system, and the schematic diagram is shown in Fig. 1. A standing-wave resonator was firstly set up to generate the 1064 nm pulse laser[18]. A fiber-coupled laser diode with a wavelength of 808 nm as well as the maximum power of 25 W acted as the pump source. The numerical aperture (NA) and the diameter of the fiber were 0.22 and 400 μm, respectively. A telescope system including two lenses with the same focal length of 30 mm was adopted to couple the pump laser beam to a spot with the waist diameter of 400 μm, which could make sure there was optimal mode-matching between the pump laser and the oscillating laser. The gain medium was an *a*-cut squared Nd:YVO_4 crystal with the cross section of 3 mm × 3 mm and the whole length of 20 mm, respectively, which contained an undoped end cap of 5 mm and a Nd-doped part of 15 mm with the doped concentration of 0.2%. To attain the stable oscillation of the 1064 nm laser, the front face of the Nd:YVO_4 crystal was coated with the anti-reflection (AR) film at 808 nm ($R_{888\,nm} < 0.5\%$) as well as the high-reflection (HR) film at 1064 nm ($R_{1064\,nm} > 99.8\%$) and was employed as the input coupler. A wedge angle of 1.5° at the rear surface coated with AR film at 1064 nm ($R_{1064\,nm} < 0.5\%$) was fabricated to suppress the σ-polarization oscillation and enhance the superiority of the π-polarization mode. The cavity mirror M_1 was a plane-concave mirror with a curvature radius of 100 mm and coated with high-transmission (HT) film at 808 nm ($T_{808\,nm} > 99\%$) and HR film at 1064 nm ($R_{1064\,nm} > 99.8\%$), respectively. The output coupler M_2 was a flat mirror and coated with partial transmission film for 1064 nm ($T = 37\%$).

A quartz acoustic-optic modulator (AOM) (I-QS041-1.5C10G-4-SO12, G&H) with the highest repetition rate of 1 MHz was used for the intra-cavity *Q*-switching operation, which could effectively generate the short-pulsed laser. The launched 1064 nm laser was reflected by a flat mirror M_3 coated with the HR film at 1064 nm and then focused on the SHG crystal LBO_I by lens f_3 with the focal length of 50 mm. A 10-mm-long type-I noncritical phase-matching LBO (S1, S2: AR at 1064 nm, 532 nm) with $\theta = 90°$, $\varphi = 0°$ was chosen as the SHG crystal since it was immune to the group velocity mismatch and the walk-off effect in the SHG process, which would keep the alignment of the fundamental-wave 1064 nm laser and the generated second-harmonic-wave 532 nm laser. Sequentially, the generated 532 nm and residual 1064 nm laser beams were collimated to 1.7 mm by lens f_4 with the focal length of 80 mm for completely covering four units of the MLA with the side length of 600 μm of every unit. The side length and thickness of the MLA_1 were 10 mm and 1 mm, respectively. The micro-structure of the MLA had a quadrilateral arrangement and is shown in Fig. 2(a). The focal length of 27 mm for every MLA unit was chosen in the experiment for achieving the maximal efficiency of the THG process. In order to reduce the loss caused by MLA_1, both surfaces were coated with AR films at 1064 nm and 532 nm ($R_{1064\,nm} < 0.2\%$; $R_{532\,nm} < 0.5\%$). With the assistance of MLA_1, the incident collimated laser beams including both 1064 nm and 532 nm lasers were successfully divided into four sub-beams and simultaneously focused at the different cross-section areas of the THG crystal. In order to keep the overlap between the 1064 nm laser and 532 nm lasers in the THG

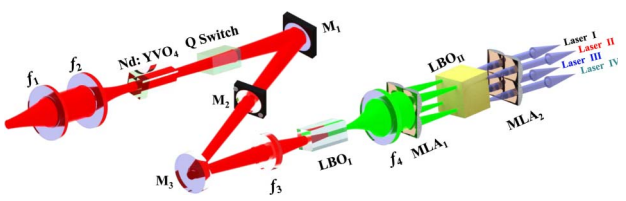

Fig. 1. Schematic diagram of the designed pulsed 355 nm UV laser with four sub-beam output.

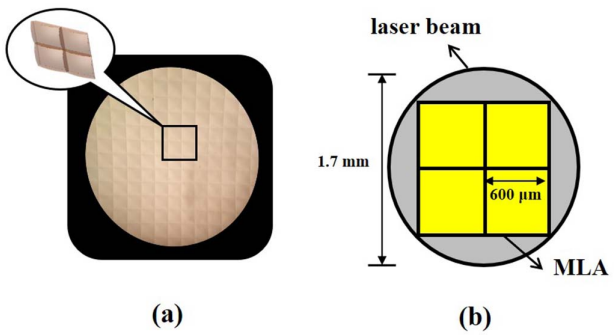

Fig. 2. (a) Microscopic images of MLA. (b) Size of the MLA and collimated laser beam.

process as much as possible, a walk-off compensated nonlinear crystal (LBO_{II}) with the wedged cut angle of 17° was employed in the experiment, which was critically type-II phase-matching LBO with the phase-matching angle of $\theta = 42.2°$, $\varphi = 90°$. Both surfaces were coated with the AR films at 1064 nm, 532 nm, and 355 nm. After LBO_{II}, another MLA (MLA_2) with the same focal length as MLA_1 was used to collimate the obtained 355 nm laser, which was necessary to prevent the interference among the generated sub-beams of the 355 nm UV laser beams.

3. Experimental Results and Discussion

In the experiment, before implementing the SHG and THG, the pulsed 1064 nm laser was firstly optimized by accurately matching the resonator length and changing the modulation frequency of the AOM. As a result, a stable pulsed 1064 nm laser with the average power of 12.1 W at the repetition rates of 46.6 kHz was attained. The measured stability and beam quality were 0.43% (rms) and $M_x^2 = 1.04$, $M_y^2 = 1.01$, respectively. Because the measured pulse width of the 1064 nm laser was 9.80 ns, the energy and the peak power of the single pulse were 0.26 mJ and 26.5 kW, respectively. Then, the 1064 nm laser beam leaked from M_2 was reflected by M_3 and focused on LBO_I by utilizing a lens with the focal length of 50 mm to realize the SHG. In order to satisfy the requirement of the THG, the output power of the 532 nm laser was optimized. When the waist radius of the 1064 nm laser inside the LBO_I was 148 μm and the temperature of LBO_I was 163.1°C, the output power of the 355 nm UV laser reached the maximum. In this case, the achieved average power of the 532 nm laser was 4.45 W along with a 6.87 W residual 1064 nm laser, which meant that only 5.23 W was converted to the 532 nm laser by the SHG. It was seen that the optimal 355 nm power was obtained at SHG conversion efficiency of 36.8% but not the highest efficiency. That is because too high conversion efficiency would lead to spatial and temporal character distortion of the 1064 nm laser beam, which would decrease the THG efficiency. In the THG process, the obtained 532 nm laser and the residual 1064 nm laser were firstly collimated into a parallel beam by lens f_4. Figure 2(b) shows the size information of the MLA and the collimated laser beam. After MLA_1, the 1064 nm laser together with the 532 nm laser was divided into four groups and injected into the THG LBO crystal, and the beam waists of the four sub-beams were about 15 μm. In the experiment, the positions of the lens and THG crystal were adjusted precisely to maximize the overlap of the 1064 nm beam and 532 nm beam to improve the efficiency. As a result, four collimated 355 nm UV laser sub-beams (Laser I, Laser II, Laser III, and Laser IV) were successfully attained at the same time after LBO_{II} and MLA_2 in the experiment. There was no 355 nm laser beam covered among the sub-beams for large extra losses for the 1064 nm and 532 nm lasers between the micro-lens units and phase-mismatching in the THG crystal. A small part of these four UV laser beams were separated and injected into a CCD camera to capture their beam profiles as well as the intensity distribution. The recorded results are illustrated in Fig. 3. It was clearly seen that all four sub-beams had distinct outlines [Fig. 3(a)] and were close to the Gaussian distribution [Fig. 3(b)] because the interference phenomenon between them was not observed, which was beneficial for the laser-processing fields. However, it was easily found that the beam profiles of Laser I, Laser II, Laser III, and Laser IV were slightly elliptical, which was mainly caused by two reasons. One was the walk-off effect; the energy flux density vector of 532 nm was not always along with its wavevector owing to the different polarization states of the 1064 nm and 532 nm lasers. The other was the imperfect Gaussian beams of the 1064 nm and 532 nm lasers because of the imperfect noncritical phase-matching of LBO_I in the generation process of the 532 nm laser. In practice, the elliptical beams can be shaped separately in X and Y directions by a cylindrical lens according to the actual needs. However, the obtained four 355 nm UV laser sub-beams are sufficient to prove the feasibility of the designed scheme we proposed in this Letter, which can pave the way to demonstrate more sub-beam laser output.

Further, after filtering the residual 1064 nm and 532 nm lasers, the output powers of the generated sub-beam 355 nm UV laser were also measured and depicted in Fig. 4. The maximal average powers of Laser I, Laser II, Laser III, and Laser IV were 269 mW, 179 mW, 217 mW, and 410 mW, respectively.

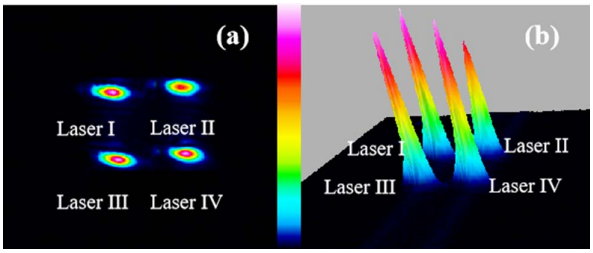

Fig. 3. Beam profiles and intensity distribution of the attained four pulsed 355 nm UV laser sub-beams.

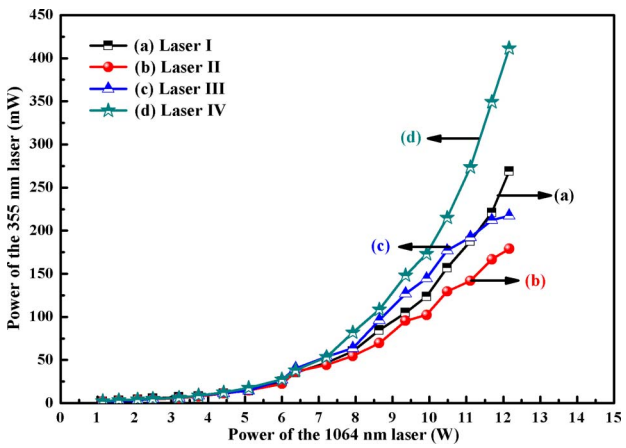

Fig. 4. Output powers of four pulsed 355 nm UV laser sub-beams versus the power of the fundamental-wave 1064 nm laser.

The total output power was 1.075 W, and the corresponding efficiency was 8.9%. As a comparison, the output power of the 355 nm laser could reach up to 3.3 W if the adopted micro-lens was replaced by a single coupling lens with the focal length of 15 mm. The corresponding efficiency was up to 27.3%. It was seen that the efficiency of the micro-lens was much lower than that of the single coupling lens, which resulted from the extra losses caused by the several nanometers dead zones among the micro-lens units and the imperfect phase-matching of four sub-beams in the THG crystal. Compared to Laser I, Laser II, Laser III, and Laser IV, it was seen that the average power of the four sub-beams was different, and Laser IV had the highest power, which resulted from the different phase-matchings for the employed critically type-II phase-matching LBO with the wedged cut angle of 17°. In practice, if the uniformity of the sub-beams is needed, we have to readjust the placement of MLA_1 and THG crystal to sacrifice total conversion efficiency and make the output powers of the four sub-beams the same. Meanwhile, there was no evidence of saturation in the output power at the maximum pump power, which meant that the output power could be further increased by increasing the pump power. On this basis, the pulse width of every sub-beam was measured by a high-speed Si photon diode (PD, DET10A/M, Thorlabs), and the transformed electrical signal from the PD was recorded by an oscilloscope with the bandwidth of 1 GHz (RTO2014, R&S). The relationship between the pulse width and the power of the 355 nm UV laser for four sub-beams are depicted in Fig. 4. It was clear that all of the pulses were quickly squeezed with the increase of the powers of the 355 nm UV lasers, which resulted from the high intensity of the fundamental-wave 1064 nm and second-harmonic-wave 532 nm lasers.

At the same time, the pulse widths of four sub-beams at the maximum output power are illustrated in the insets of Figs. 5(a)–5(d). We also found that the pulse widths were 8.53 ns with a rising time of 3.88 ns and falling time of 10.43 ns for Laser I, 8.23 ns with the rising time of 3.90 ns and falling time of 10.25 ns for Laser II, 8.90 ns with the rising time of 3.98 ns and falling time of 10.83 ns for Laser III, and 8.52 ns with the rising time of 3.90 ns and falling time of 10.56 ns for Laser IV, respectively. It revealed that there were some differences between the four sub-beams, but the pulse widths of all the sub-beams were shorter than 9 ns. Therefore, the pulse peak powers of four sub-beams were up to 0.68 kW, 0.47 kW, 0.52 kW, and 1.04 kW, respectively.

In the experiment, the stable pulse repetition rate and good symmetry of the pulse in geometry morphology were observed, which would make the obtained laser suitable for industrial processing. In addition, the beam quality factors (M^2) of these generated four sub-beam pulsed 355 nm UV lasers were separately measured by a beam quality meter (S-WCD-UCD12-UV, DataRay Inc.). The measured results are shown in Fig. 6. For Laser I, Laser II, Laser III, and Laser IV, the measured values of M_x^2 and M_y^2 were 1.60 and 1.09, 2.33 and 1.90, 2.70 and 1.32, 2.41 and 1.17, respectively. Actually, it was expected that the

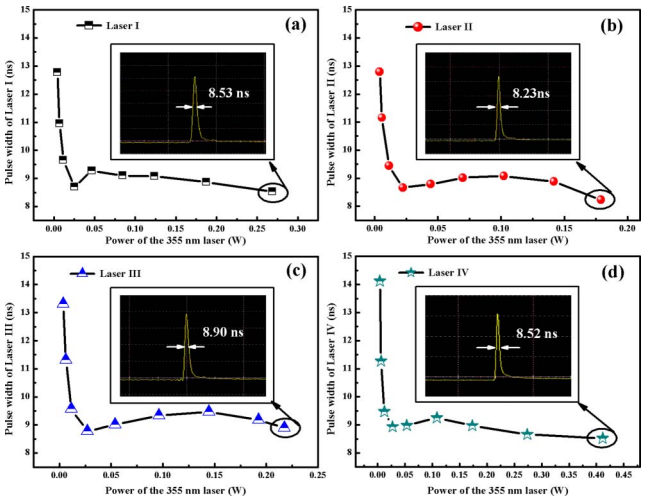

Fig. 5. Pulse width variations of the four 355 nm UV laser sub-beams and the pulse width at the maximal power. (a) Laser I, (b) Laser II, (c) Laser III, and (d) Laser IV.

excellent Gaussian beams would be attained by using a micro-cylindrical lens array as the component of the laser beam shaping. At the same time, after one month of continuous operation of the laser, we found that the power of every sub-beam of the attained laser did not decrease substantially. Eventually, the power stability in 12 h of Laser IV (410 mW) was typically recorded after one month since it had the highest power among the four generated sub-beams. The results are shown in Fig. 7. The power stability of Laser IV was 0.6% (rms), which was significantly better than that of the commercial product (rms ≤ 3%)[19]. The inset of Fig. 7 gives the short-term power fluctuation of Laser IV, 9.7 mW in 30 min. In addition, we examined the THG crystal with a stereo microscope, which found that there was not any damage in the crystal. All of these predicted that the generated four-beam pulsed 355 nm UV laser based on

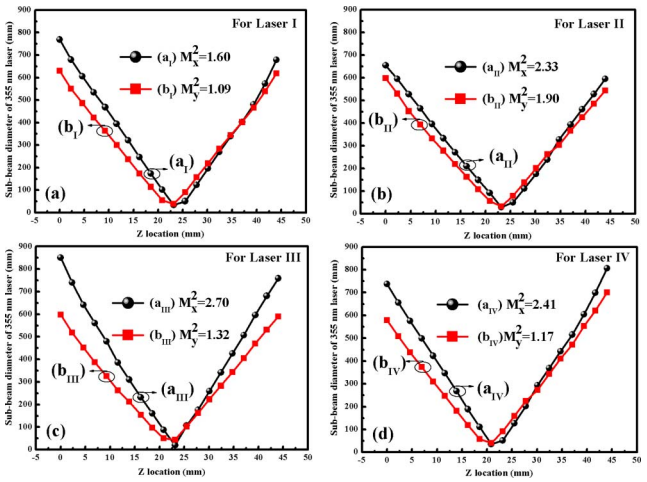

Fig. 6. M^2 of every sub-beam of the generated pulsed 355 nm UV laser.

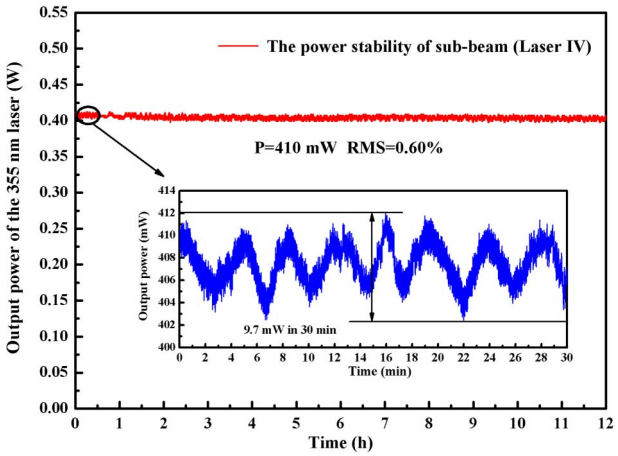

Fig. 7. Power stability of Laser IV for 12 h.

MLA had excellent power stability owing to the decrease of power density of the 355 nm laser inside the THG crystal.

4. Summary

In summary, a compact and stable multi-beam pulsed 355 nm UV laser source based on an MLA was reported for the first time, to the best of our knowledge, which can not only directly generate multi-beam UV laser output, but also effectively improve the lifetime of the attained UV laser. The maximal average powers of 269 mW (Laser I), 179 mW (Laser II), 217 mW (Laser III), and 410 mW (Laser IV) for 355 nm UV lasers were attained at the repetition rates of 46.6 kHz. The measured pulse widths were 8.53 ns (Laser I), 8.23 ns (Laser II), 8.90 ns (Laser III), and 8.52 ns (Laser IV), corresponding to the pulse peak powers of 0.68 kW, 0.47 kW, 0.52 kW, and 1.04 kW, respectively. The M^2 value and the power stability of the four sub-beams were measured in the experiment. Especially, there was no power decrease to be found in the long-term measurement for four sub-beam 355 nm UV lasers, which showed that the obtained multi-beam pulsed 355 nm UV laser could be used in laser processing, and the proposed method for multi-beam UV laser generation could effectively improve the lifetime of the employed THG crystal and obtained UV laser.

Acknowledgement

This study was supported by the National Natural Science Foundation of China (Nos. 61975100 and 62027821), Program for the Innovative Talents of High Education Institutions of Shanxi, and Fund for Shanxi "1331 Project" Key Subjects Construction.

References

1. J. Bovatsek, A. Tamhankar, and R. Patel, "UV lasers improve PCB manufacturing processes," Laser Focus World **48**, 48 (2012).
2. R. S. Patel, A. Tamhankar, and T. Edwards, "Diode-pumped solid-state UV lasers improve LED sapphire wafer scribing," Photon. Spectra **44**, 46 (2010).
3. T. Rauch, R. Delmdahl, V. Pfeufer, and M. Mondry, "Advanced UV lasers enable precision processing," Laser Tech. J. **6**, 20 (2009).
4. Z. Kuang, W. Perrie, D. Liu, P. Fitzsimons, S. P. Edwardson, E. Fearon, G. Dearden, and K. G. Watkins, "Ultrashort pulse laser patterning of indium tin oxide thin films on glass by uniform diffractive beam patterns," Appl. Surf. Sci. **258**, 7601 (2012).
5. D. Ashkenasi, A. Rosenfeld, H. Varel, M. Wahmer, and E. E. B. Campbell, "Laser processing of sapphire with picosecond and sub-picosecond pulses," Appl. Surf. Sci. **120**, 65 (1997).
6. A. Wolynski, T. Herrmann, P. Mucha, H. Haloui, and J. L'huillier, "Laser ablation of CFRP using picosecond laser pulses at different wavelengths from UV to IR," Phys. Procedia **12**, 292 (2011).
7. C. T. Chen, Y. C. Wu, A. D. Jiang, B. C. Wu, G. M. You, R. K. Li, and S. J. Lin, "New nonlinear-optical crystal: LiB_3O_5," J. Opt. Soc. Am. B **6**, 616 (1989).
8. B. C. Wu, N. Chen, C. T. Chen, D. Q. Deng, and Z. Y. Xu, "Highly efficient ultraviolet generation at 355 nm in LiB_3O_5," Opt. Lett. **14**, 1080 (1989).
9. H. Chen, Q. Liu, P. Yan, and M. Gong, "High-power 355 nm ultraviolet lasers operating at ultrahigh repetition rate," Laser Phys. Lett. **10**, 025401 (2013).
10. L. Zhang, K. Li, D. G. Xu, H. J. Yu, G. C. Zhang, Y. Y. Wang, L. R. Wang, F. X. Shan, C. Yan, Y. Y. Yang, B. H. Wang, N. Wang, X. C. Lin, Y. C. Wu, and J. Q. Yao, "A 7.81 W 355 nm ultraviolet picosecond laser using $La_2CaB_{10}O_{19}$ as a nonlinear optical crystal," Opt. Express **22**, 17187 (2014).
11. S. C. Kumar, E. S. Bautista, and M. Ebrahim-Zadeh, "Stable, high-power, Yb-fiber-based, picosecond ultraviolet generation at 355 nm using BiB_3O_6," Opt. Lett. **40**, 403 (2015).
12. B. Xu, Z. Y. Hou, M. J. Xia, L. J. Liu, X. Y. Wang, R. K. Li, and C. T. Chen, "High average power third harmonic generation at 355 nm with $K_3B_6O_{10}Br$ crystal," Opt. Express **24**, 10345 (2016).
13. S. Möller, Ä. Andresen, C. Merschjann, B. Zimmermann, M. Prinz, and M. Imlau, "Insight to UV-induced formation of laser damage on LiB_3O_5 optical surfaces during long-term sum-frequency generation," Opt. Express **15**, 7351 (2007).
14. H. L. Hong, Q. Liu, L. Huang, and M. L. Gong, "Improvement and formation of UV-induced damage on LBO crystal surface during long-term high-power third-harmonic generation," Opt. Express **21**, 7285 (2013).
15. J. Xiang, J. X. Li, H. Li, C. Y. Zhang, Q. F. Dai, S. L. Tie, and S. Lan, "Polarization beam splitters, converters and analyzers based on a metasurface composed of regularly arranged silicon nanospheres with controllable coupling strength," Opt. Express **24**, 11420 (2016).
16. P. G. Luan and K. D. Chan, "Transmission characteristics of finite periodic dielectric waveguides," Opt. Express **14**, 3263 (2006).
17. Y. F. Ma, Y. He, X. Yu, X. D. Li, J. Li, R. P. Yan, J. B. Peng, X. L. Zhang, R. Sun, Y. B. Pan, and D. Y. Chen, "Multiple-beam, pulse-burst, passively Q-switched ceramic Nd:YAG laser under micro-lens array pumping," Opt. Express **23**, 24955 (2015).
18. F. Q. Li, Y. H. Zheng, and K. S. Zhang, "An all-solid-state high power cw Nd:YVO_4/LBO green laser of TEM_{00} operation," J. Quantum Opt. **12**, 176 (2006).
19. https://www.huaraylaser.com/productinfo/589050.html.